Available online at www.sciencedirect.com
ScienceDirect
Ocean Modelling 22 (2008) 48–65
Ocean Modelling
www.elsevier.com/locate/ocemod

Relative dispersion from a high-resolution coastal model of the Adriatic Sea

Angelique C. Haza [a,*], Andrew C. Poje [b], Tamay M. Özgökmen [a], Paul Martin [c]

[a] RSMAS/MPO, University of Miami, Miami, FL, USA
[b] Department of Mathematics, College of Staten Island, CUNY, Staten Island, USA
[c] Naval Research Laboratory, Stennis Space Center, MS, USA

Received 22 August 2007; received in revised form 10 January 2008; accepted 11 January 2008
Available online 6 February 2008

Abstract

Synthetic drifter trajectories computed from velocity data produced by a high-resolution NCOM model are used to investigate the scaling of relative dispersion and the distribution of finite-scale Lyapunov exponent (FSLE) fields in the Adriatic Sea. The effects of varying degrees of spatial and temporal filtering of the input Eulerian velocity fields on the Lagrangian statistics are investigated in order to assess the sensitivity of such statistics to model error. It is shown that the relative dispersion in the model Adriatic circulation is generally super-diffusive, scaling nearly ballistically in close agreement with Lagrangian observations from a limited set of drifters. The large-scale dispersion is dominated by persistent separation regions and the controlling influence of the Western Adriatic Current (WAC). Temporal filtering with averaging windows up to monthly time scales only affects the relative dispersion at scales smaller than 20 km without altering the overall scaling regime. In contrast, spatial smoothing at scales as small as 5 km significantly reduces relative dispersion at all scales up to 100 km. While basin-scale dispersion statistics are strongly dependent on spatial resolution of the model WAC, maps of FSLE fields over initial conditions indicate that the detailed geometry of the dispersion is determined to a large extent by the temporal resolution of the model. In addition, the degree of spatial heterogeneity in the flow field implies that the existence, or non-existence, of a distinct exponential regime in the FSLE at small scales is extremely sensitive to the details of particle pair sampling strategies.
Published by Elsevier Ltd.

1. Introduction

The transport, spreading, and mixing of passive particles and tracers have a wide range of practical applications in both classical and geophysical fluid flows. These include the spreading of industrial plumes in the air, of pollutants, discharges, and fish larvae in the ocean, or global advection of temperature and tracers in the ocean thermohaline circulation. The Lagrangian framework

$$\frac{\mathrm{d}\mathbf{x}}{\mathrm{d}t} = \mathbf{v}(t) = \mathbf{u}(\mathbf{x}, t) \tag{1}$$

is the natural setting for such problems, where $\mathbf{x}$ is the position, $\mathbf{v}$ is the velocity of the Lagrangian particle, and $\mathbf{u}$ is the velocity field of the underlying Eulerian flow.

Many of the above-mentioned practical applications can be thought of in terms of the advection of a cluster of Lagrangian particles with the flow field. One of the metrics that can be used to describe this problem is the absolute (or single-particle) dispersion

$$A^2(t, t_0) = \frac{1}{N}\sum_{i=1}^{N} |\mathbf{x}_i(t) - \mathbf{x}_i(t_0)|^2 = \langle |\mathbf{x}_i(t) - \mathbf{x}_i(t_0)|^2 \rangle, \tag{2}$$

which quantifies the average distance covered in time by N Lagrangian particles following their release at $t = t_0$.

Another Lagrangian metric more closely tied to scalar mixing processes is the relative (two-particle) dispersion

$$D^2(t) = \langle |\mathbf{x}^{(1)}(t) - \mathbf{x}^{(2)}(t)|^2 \rangle, \tag{3}$$

where the average is over all pairs of particles in the cluster. Thus, relative dispersion quantifies the mean-square particle separation and is the focus of the present study.

* Corresponding author. Tel.: +1 786 546 1285.
E-mail address: ahaza@rsmas.miami.edu (A.C. Haza).

1463-5003/$ - see front matter Published by Elsevier Ltd.
doi:10.1016/j.ocemod.2008.01.006

The interpretation of relative dispersion defined in (3) is often obscured in the presence of intermittent turbulence and finite-sized domains (Boffetta et al., 2000). The root cause of this is that the average in (3) is taken over a wide range of separation scales at any one time and is thus dominated by those particle pairs with the largest separations. To address this, a complementary measure, namely the finite-scale Lyapunov exponent (FSLE), is often employed (Artale et al., 1997; Aurell et al., 1997)

$$\lambda(\delta) = \frac{\ln(\alpha)}{\langle \tau(\delta) \rangle}, \tag{4}$$

where $\langle \tau(\delta) \rangle$ is the averaged time (over the number of particle pairs) required to separate from a distance of δ to $\alpha\delta$. Like Richardson's original time–distance graphs (Richardson, 1926), the FSLE provides a measure of dispersion as a function of the spatial scale and serves to isolate the different dispersion regimes corresponding to the different scales of the oceanic flows. Spatial distributions of the FSLE and related measures such as finite-time Lyapunov exponents have recently been used to define so-called *Lagrangian coherent structures* (Shadden et al., 2005) and to map transport barriers and mixing regimes in a number of oceanic applications (Abraham and Bowen, 2002; d'Ovidio et al., 2004; Waugh et al., 2006; Olascoaga et al., 2006).

The study of relative dispersion in fluid flows is a fundamental area of research, dating back to the 1920s. The reader is referred to Bennett (1987) and Sawford (2001) for a comprehensive review of the subject matter. Here, a short summary of this material is provided followed by how the present study is motivated and why it is original in the context of oceanic flows.

Traditionally, relative dispersion has been related to turbulent cascade processes in the Eulerian velocity field (Bennett, 1984; Piterbarg, 2005). The original formula proposed by Richardson (1926), $D^2(t) = C\epsilon t^3$, where $C = O(1)$ is a constant and ϵ is the turbulent kinetic energy dissipation rate, is found to be consistent with Kolmogorov's (1941) energy-cascade law for three-dimensional (3D), homogeneous, isotropic turbulence in the inertial range, $E(k) \sim \epsilon^{2/3} k^{-5/3}$ (Batchelor, 1952). Nevertheless, the precise mechanisms responsible for Richardson's (1926) relation and the range of conditions under which it is valid remains the subject of some debate even in idealized experimental and numerical settings (e.g., Bourgoin et al., 2006). The direct applicability to oceanic flows, which tend to be two-dimensional (2D) under the effects of rotation and stratification (Cushman-Roisin, 1995) and which are often dominated by persistent inhomogeneity and anisotropy, is open to question. Kraichnan (1967) proposed that the simplest 2D turbulence can exhibit a dual spectrum, namely an enstrophy cascade $E(k) \sim \beta^{2/3} k^{-3}$, where β is the enstrophy dissipation at scales smaller than the forcing scale, $k > k_f$, and an inverse energy-cascade $E(k) \sim \epsilon^{2/3} k^{-5/3}$ at scales larger than the forcing scale, $k < k_f$. In the enstrophy cascade regime, exponential particle separation can be expected, $D^2(t) = D_0^2 \exp(\lambda_0 t)$, where λ_0^{-1} is the enstrophy cascade time scale (Lin, 1972). Note that the emergence of a dual spectrum in 2D turbulence requires forcing at a narrow range of scales and the spectrum tends toward $E(k) \sim k^{-3}$ for the more typical oceanic case of broad-band forcing (Lesieur, 1997). At the asymptotic limit of very long times and particle separations, when all particle correlations diminish, the so-called diffusive regime, $D^2(t) = 2\kappa t$, where κ is the diffusivity coefficient, should be attained (Taylor, 1921).

Recent developments in the understanding of Lagrangian transport and mixing (Wiggins, 2005) indicate that there are issues other than turbulent cascades that deserve consideration for understanding oceanic relative dispersion. Of particular importance is the concept of chaotic advection, in which (laminar) Eulerian flow fields with relatively simple spatial structure can lead to complex Lagrangian behavior due to the effect of time dependence alone (Aref, 1984). Chaotic flows, by their very definition, lead to exponential particle separations for small initial displacements.

Finally, various empirical correlations have been established between the Lagrangian relative dispersion and the type of coherent structures in the Eulerian fields. For instance, the ballistic regime, $D^2(t) \sim t^2$, is observed in the presence of persistent correlations and shear dispersion (Iudicone et al., 2002) and the sub-diffusive regime, $D^2(t) \sim t^\gamma$ with $\gamma < 1$, is often attributed to particle trapping within eddies (Cardoso et al., 1996; Provenzale, 1999).

While it is possible to parse further the spatial and temporal scales into other regimes of dispersion on a theoretical basis (Sawford, 2001; Piterbarg, 2005), there appears to be a high degree of uncertainty about which regimes are actually attained in practice, namely in the laboratory, atmospheric and oceanic observations, and numerical simulations. Each one of these methods introduces various factors that can cause deviations from theory. For instance, the Reynolds number, thus the range of the interacting turbulent processes, tends to be limited in laboratory experiments and direct numerical simulations in comparison to that in the real ocean. Also, the ocean is subject to a very complex forcing at the surface, the presence of strongly inhomogeneous mean currents, and the limiting effects of the boundaries. These effects are expected to lead to deviations of relative dispersion from the regimes that are expected on the basis of theory. As such, a brief review of the observational experience follows.

In laboratory experiments of 2D homogeneous turbulence, Julien (2003) reported a clear exponential separation regime. Bourgoin et al. (2006) obtained Batchelor (1952) scaling (similar to ballistic) in 3D homogeneous turbulence in the laboratory, but could not confirm the Richardson regime. Numerical simulations of 2D homogeneous turbulence (Boffetta and Celani, 2000; Bracco et al., 2004) yielded both the exponential and Richardson regimes. Boffetta and Sokolov (2002), using 3D direct numerical simulations of homogeneous turbulence, emphasized that deviations from the Richardson regime is a consequence

of turbulence intermittency. Balloon experiments in the atmosphere exhibited an exponential regime at short separations (Morel and Larcheveque, 1974; Er-El and Peskin, 1981) and different regimes at larger scales such as the diffusive law (Morel and Larcheveque, 1974) or a mixed regime between the ballistic and Richardson laws (Er-El and Peskin, 1981), while the Richardson regime is observed by Lacorata et al. (2004) for separations in the 100–1000 km range, followed by a diffusive regime. Experiments with an atmospheric global circulation model showed all three regimes: exponential, ballistic, and Richardson, depending on the latitude (Huber et al., 2001).

The investigations of relative dispersion in the ocean are relatively few. While thousands of drifters have been released during the WOCE (World Ocean Circulation Experiment), the number of drifter launches that are near-simultaneous and in close proximity is very small. As such, this large data set is not suitable for a systematic investigation of relative dispersion in the ocean. Several process-oriented ocean experiments have been conducted. Most notably, LaCasce and Bower (2000) estimated relative dispersion from sub-surface floats released during several observational programs in the North Atlantic. They found a diffusive regime in the eastern part of the domain and a Richardson regime in the western part of the domain that was attributed to an inverse turbulent cascade of energy. The exponential regime, as expected from the enstrophy cascade and/or chaotic advection, was not resolved, possibly because the initial pair separations were too large. LaCasce and Ohlmann (2003) revisited this problem using the rich drifter data set in the Gulf of Mexico. They found an exponential regime for particle separations between 1 and 40–50 km, and a mixture of ballistic and Richardson regimes up to scales of several hundred kilometers. Lacorata et al. (2001) show a mixed regime between ballistic and Richardson for spatial scales of 40–200 km using drifters released in the Adriatic Sea. Ollitrault et al. (2005) used another set of sub-surface floats in the North Atlantic and documented a brief exponential regime followed by a Richardson's regime for separation distances between 40 and 300 km and a diffusive regime for larger separations.

The study of relative dispersion using ocean models is surprisingly limited as well. Using multi-layer, quasi-geostrophic, double-gyre simulations, Berloff et al. (2002) and Berloff and McWilliams (2002) found a zonal asymmetry consistent with the results of LaCasce and Bower (2000), ranging from a diffusive regime at the eastern to a ballistic regime at the western boundaries. Iudicone et al. (2002) used a realistic, eddy-permitting ($\Delta x = 25$ km) circulation model of the Mediterranean Sea and reported an exponential regime at meso-scales and a ballistic regime up to sub-basin scales. They have also found that, while uncertainties in time sampling of drifter trajectories lead to differences at small scales, the large-scale dispersion remains robust. Similar findings are reported by Bracco et al. (2004) who find extremely small differences in relative dispersion results in a comparison of three-dimensional, quasi-geostrophic turbulence and similar slices of two-dimensional, barotropic flows.

The main objective of the present study is to contribute to this on-going, long-standing debate on the classical problem of relative dispersion, particularly given the relatively small number of studies that have been conducted directly on ocean flows. This study has two novel aspects. First, we analyze synthetic drifter trajectories from the Navy Coastal Ocean Model (NCOM) with high-resolution (1 km) and realistic wind, river outflow, tidal, and atmospheric forcings. The model has been shown to lead to accurate analyses on the basis of operational programs conducted in the Adriatic Sea (Martin et al., 2006; Haza et al., 2007). The Adriatic circulation provides a relatively extreme case of a bounded ocean flow dominated by coherent features including intense boundary currents and separation regions and, in this sense, is quite far removed from a homogeneous or isotropic turbulence. Second, the relatively fine spatial and temporal model resolution allows us to address questions of scale dependence and velocity sampling in the determination of model Lagrangian statistics. As discussed by Iudicone et al. (2002), there is an increasing emphasis on Lagrangian analyses of OGCM output. Such analyses are typically conducted *off-line* with sub-sampled time slices of previously computed Eulerian model velocity fields. Also, remotely sensed altimetry data are often analyzed to construct approximate velocity fields for the purpose of Lagrangian analyses. The observations necessarily result in some degree of both spatial and temporal smoothing. Questions concerning the effects of temporal and spatial filtering of the input Eulerian velocity on the resulting Lagrangian structures and statistics can be addressed in the context of a single high-resolution model such as the one considered here.

In this paper, we address three main questions:

- What are the regimes of relative dispersion in the Adriatic Sea, based on a high-resolution coastal ocean model?
- How are these dispersion regimes modified as a result of uncertainties in the Eulerian velocity field as represented by their spatial and temporal smoothing?
- What are the spatial patterns of relative dispersion in the model Adriatic and how robust are these distributions to perturbations in the input Eulerian velocity fields?

It is also worth noting that spatial averaging affects the turbulent wave-number spectrum, while time averaging reduces the variability of the Eulerian field. As such, a fourth objective of this study is to make progress towards resolving the question of the relative importance of turbulent cascade processes versus chaotic advection arising from the time variability of coherent flow features on the behavior of the relative dispersion.

The paper is organized as follows: the numerical model is described in Section 2, the Lagrangian tools are defined in Section 3, results for the full field and filtered velocities

are presented in Section 4, and the main results are summarized in Section 5.

2. Coastal model and configuration

The ocean model used for this study is the NCOM as described in Martin (2000), with some improvements as described in Morey et al. (2003) and Barron et al. (2006). This is a hydrostatic model, which is similar in its physics and numerics to the Princeton Ocean Model (POM) (Blumberg and Mellor, 1987), but uses an implicit treatment of the free surface and a hybrid vertical grid with sigma coordinates in the upper layers and (optionally) level coordinates below a user-specified depth.

The model equations include a source term that can be used for river inflows. A third-order upwind method (Holland et al., 1998) was used for advection. Vertical mixing was computed using the Mellor–Yamada Level 2 scheme (Mellor and Yamada, 1974). The equation of state used was that of Mellor (1991).

The ocean model domain consists of the entire Adriatic Sea, a sub-basin of the Mediterranean Sea, and it includes the Strait of Otranto and a small part of the northern Ionian Sea. The setting of the model for the Adriatic Sea is described in detail in Martin et al. (2006). The horizontal grid resolution is 1019.5 m. The vertical grid consists of 32 total layers, with 22 sigma layers used from the surface down to a depth of 291 m and level coordinates used below 291 m. Hence, the grid is like a regular sigma coordinate grid in water shallower than 291 m and similar to a level grid in deeper water. The vertical grid is uniformly stretched from the surface downward with a maximum thickness of the upper layer of 2 m and a maximum depth of 1262 m.

Initial conditions and daily boundary conditions were taken from a hind-cast of a global model (Barron et al., 2004). The numerical treatment of the boundary conditions includes the Flather radiation condition (Flather and Proctor, 1983) for the surface elevation and depth-averaged normal velocity, Orlanski radiation conditions (Orlanski, 1976) for the tangential velocities and scalar fields, and a relaxation to the temperature and salinity from the global model near the open boundary. Tidal forcing was provided using tidal elevation and depth-averaged normal and tangential velocities at the open boundaries from the Oregon State University (OSU) tidal data bases, which are derived from satellite altimetry data (Egbert and Erofeeva, 2003). Data from the OSU Mediterranean tidal data base were used for the K1, O1, M2, and S2 constituents and data from the OSU global data base were used for P1, Q1, K2, and N2. Tidal potential forcing for these eight constituents was used in the interior of the model domain.

Atmospheric forcing was obtained from the Coupled Ocean/Atmosphere Meso-scale Prediction System (COAMPS) (Hodur, 1997). The COAMPS setup for the Adriatic consists of a triply nested grid with resolutions of 36, 12, and 4 km (Pullen et al., 2003). The outer grid of this nested grid system covers most of Europe and the Mediterranean and the inner 4-km grid covers the entire Adriatic and part of the Tyrhennian Sea. COAMPS itself is nested within the Navy Operational Global Atmospheric Prediction System (NOGAPS) (Rosmond et al., 2002). River and runoff inflows for the Adriatic were taken from the monthly climatological data base of Raicich (1996). This data base includes discharges for about 39 rivers and runoff inflows along a number of sections of the Adriatic coastline. Raicich's monthly climate values were used for all the inflows, except that daily observed discharge values were used for the Po River (Rich Signell, personal communication).

This model configuration has shown good agreement with tidal and de-tided ADCP current observations and reproduced some of the observed temperature and salinity spatial profiles (Martin et al., 2006). Additionally, the model response to Bora wind events displayed the usually observed pattern of cyclonic and anticyclonic gyres.

This model is appropriate for the present study for two main reasons. First, a recent operational experiment aimed at targeted release of drifters in high dispersion regions in the Adriatic Sea using the same model configuration showed the ability of NCOM to reproduce many aspects of the meso-scale circulation in real time (Haza et al., 2007). Second, the high spatial and temporal resolution of the model combined with a rich variety of forcing mechanisms and internal coastal flow dynamics lead to a surface velocity field exhibiting features at a wide range of scales and with high temporal variability.

A snapshot of the velocity field in the full numerical domain is depicted in Fig. 1a. The reader is referred to Poulain (1999, 2001), Cushman-Roisin et al. (2001, 2007), Falco et al. (2000), Maurizi et al. (2004) and Martin et al. (2006) for a comprehensive discussion of the circulation features and data sets. The main point is that the NCOM simulation employed here adequately approximates the main features of the upper circulation in the Adriatic Sea.

3. Experimental setup

The bulk of the results that follow concern the dispersion statistics of synthetic drifters advected for 30–60 days using the NCOM surface velocity field of September and October 2002. Throughout, we use a standard, fourth-order, Runge–Kutta scheme to solve the Lagrangian equations with an integration time-step of $\Delta t = 1$ h corresponding to the model archive time. Spatial interpolation is achieved by a third-order polynomial routine.

A subset of particle trajectories is displayed in Fig. 1b; they describe the cyclonic circulation of the Adriatic Sea corresponding to the Western and Eastern Adriatic Currents (WAC and EAC, respectively), including three other cyclonic gyres within the main cyclonic circulation. The velocities of the boundary currents (in particular the WAC) are of the order of 50–100 cm/s (as seen in the snapshot of the surface velocity field in Fig. 1a), while those of

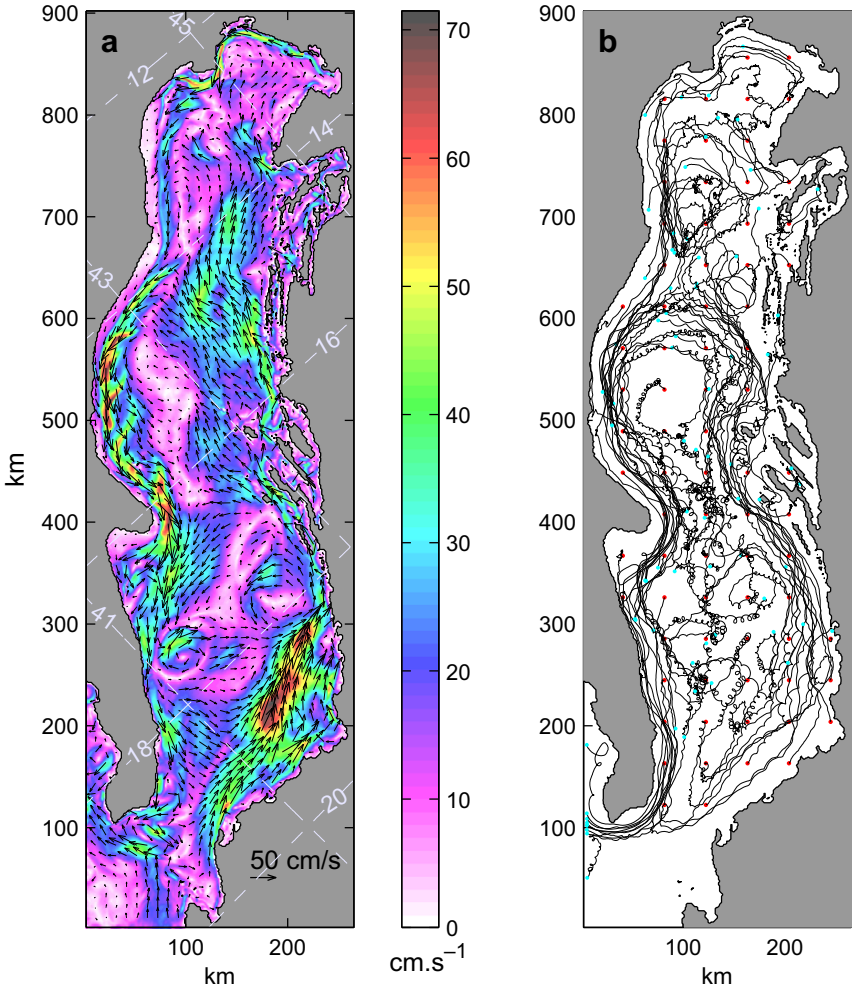

Fig. 1. (a) Snapshot of the raw NCOM surface velocity field. (b) One-month long trajectories of a subset of 74 particles advected with the NCOM velocity field corresponding to September 2002.

the Adriatic interior are ~10–20 cm/s depending on the surface winds. In the regions away from the boundary currents, the trajectories display loops with radii of 1–2 km, indicating the presence of inertial oscillations. Perhaps the most striking feature of the trajectories from Fig. 1b is the degree of control exerted by the strong boundary currents, with large transport in the longitudinal direction and relatively limited cross-basin exchange.

Given the need to adequately sample the large degree of spatial inhomogeneity in the Adriatic model and the desire to accurately map the scale-dependence of the drifter dispersion across the complete range of available model length scales, we consider two distinct initial launch grids and their corresponding statistical sampling strategies. First, a relatively dense array of drifters is initialized on a uniform regular grid with 5.1 km spacing. This corresponds to a total of $N = 5172$ drifters, placing an upper bound of $N(N-1)/2 \sim 13 \times 10^6$ possible drifter pairs from which to compute statistics. The second configuration is composed of $M = 5N$ drifters initialized in N crosses with separation $\Delta x \sim 1$ km centered on the original N launch locations. In this case, only the statistics of the fixed number of particle pairs with initial separation $D_0 = \Delta x$ are considered.

As mentioned in Section 1, both temporal and spatial filterings are applied to the Eulerian velocity fields, with the objective of not only assessing the importance of uncertainties in the input velocities on the relative dispersion, but also for examining the role of turbulent cascade processes versus chaotic advection. The temporal filtering of the flow is conducted by locally averaging the velocity field over time-windows of varying duration. For a time window given by $T = M\Delta t$, the filtered velocity u^{Ft} at location i,j and time $t = k\Delta t$ is

$$u^{Ft}_{i,j}(k) = \frac{1}{M}\sum_{m=k-M/2}^{m=k+M/2} u_{i,j}(m). \tag{5}$$

The spatial filtering of the flow is carried out via a convolution product of the velocity field with a Gaussian function. The spatially filtered velocity u^{Fs} at location i_0,j_0 and time t is

$$u_k^{\mathrm{Fs}}(i_0,j_0)=\frac{\sum_{i,j}u_k(i,j)\mathrm{e}^{[(i-i_0)^2+(j-j_0)^2]/\sigma^2}}{\sum_{i,j}\mathrm{e}^{[(i-i_0)^2+(j-j_0)^2]/\sigma^2}}. \quad (6)$$

This corresponds to a Gaussian-weighted, spatially averaged smoothing of the horizontal gradients of the flow with a length scale $\sim 2\sigma$, while preserving the time dependence. The convolution (6) is carried out with $\sigma = 0.5; 1; 2.5; 5; 10; 20$ (approximately in kilometer, since the horizontal grid spacing is ~ 1 km).

4. Results

4.1. Dispersion from the unfiltered velocity field

Relative dispersion is first calculated from the trajectory ensemble obtained from the raw (unfiltered) velocity field using the complete set of $N = 5172$ synthetic drifters and all possible drifter pair combinations. The anisotropy of dispersion is well known in the Adriatic Sea (Falco et al., 2000; Lacorata et al., 2001). As such, the relative dispersion is calculated in the zonal and meridional directions separately. Fig. 2 shows the relative dispersion curves based on trajectories with the original launch spacing of $D_0 = 5.1$ km. The relative dispersion curves are fairly well behaved due to the large number of synthetic drifter pairs included in the calculation, amounting to more than 9800 pairs initially, and down to about 6500 pairs at the end of the 2-month experiment. For times longer than a few days, relative dispersion in the meridional direction is best approximated by a t^2 growth, whereas relative dispersion in the zonal direction shows significantly slower growth, scaling approximately like $t^{1.3}$. The total relative dispersion scales as $D^2(t) \sim t^{1.9}$. Such a super-diffusive or nearly ballistic regime is typically associated with shear dispersion (Iudicone et al., 2002; LaCasce and Ohlmann, 2003) and persistent velocity correlations. Both effects are clearly evidenced in the Adriatic Sea circulation due to the presence of boundary currents (Fig. 1). As the direction of the boundary currents is imposed by the morphology of the Adriatic coastline, the similar power laws of $D^2(t)$ and $D_y^2(t)$ indicate that the relative dispersion is enhanced along the main axis of the Adriatic basin. For times longer than a month, relative dispersion in both directions slows down considerably to a sub-diffusive regime of $t^{0.7}$. This regime corresponds to dispersion at scales comparable to the basin size (Artale et al., 1997).

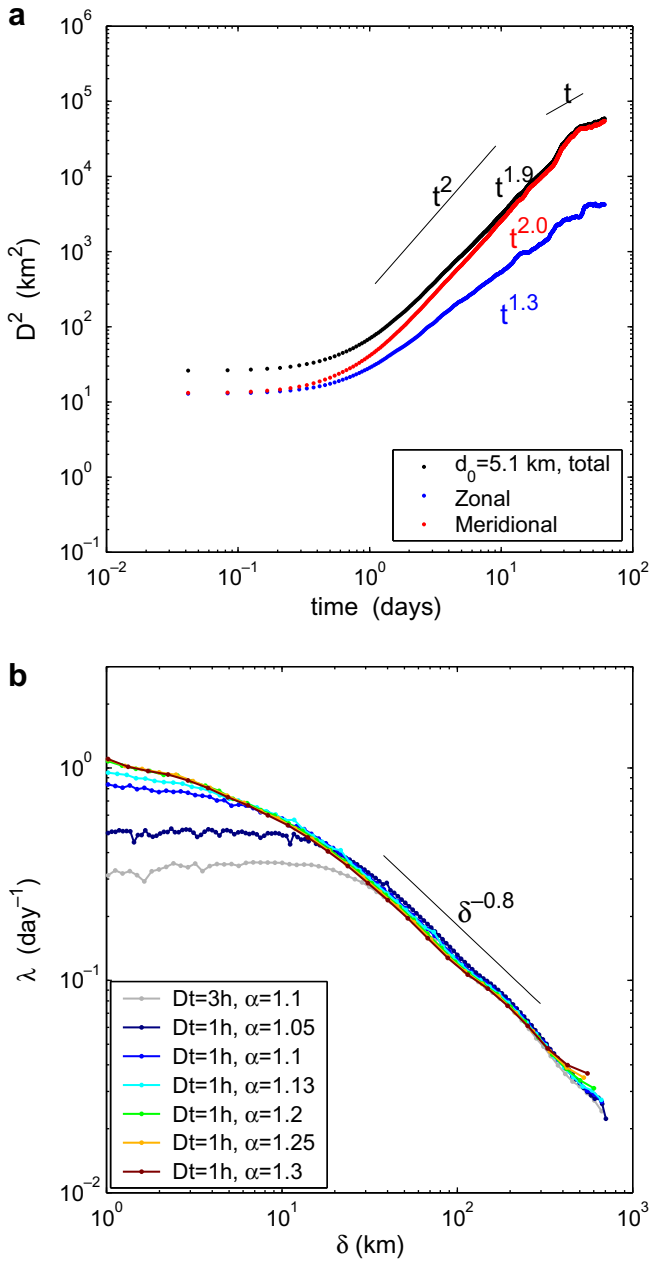

Fig. 2. (a) Relative dispersion $D^2(t)$ of the raw field computed in the zonal and meridional directions from the synthetic trajectories with original initial release distance of $D_0 = 5.1$ km. (b) Sensitivity of FSLE, $\lambda(\delta)$, to the time step Δt and parameter α for the same set of synthetic drifter trajectories.

Relative dispersion as a function of separation distance can be quantified naturally using the FSLE. While it is generally true that the FSLE defined by Eq. (4) is insensitive to the choice of the parameter α numerical and statistical considerations dictate the range of this number in applications. The minimum value of α is set by the temporal resolution Δt of the trajectories such that the time required for particle pairs to disperse from δ_0 to $\alpha\delta_0$ be longer than Δt. Thus, $\alpha\delta_0 - \delta_0 > \Delta t \Delta v$, where Δv is the velocity difference between particles in a pair. This leads to $\alpha_{\min} = 1 + \Delta t \Delta v/\delta_0$. In this experiment, $\Delta t = 1$ h, $\delta_0 = 1$ km, and an estimate of $\Delta v \sim 3$ km/day given by the Lagrangian structure function computed from the synthetic trajectories at the minimum scale of $\delta = 1$ km. Therefore, $\alpha_{\min} \approx 1.16$ is the estimated minimum value for accurate calculation of the FSLE.

Fig. 2b displays plots of $\lambda(\delta)$ for various values of α in the range of $1.05 \leqslant \alpha \leqslant 1.3$. The FSLE curves collapse for $\alpha \geqslant 1.2$, in agreement with the above estimate. There is an increasing flattening of the FSLE curves at scales

smaller than 10 km for $\alpha \leqslant 1.13$, ultimately leading to a spurious exponential regime. The length of the exponential regime for $\alpha < \alpha_{\min}$ is further enhanced if the velocity field is sub-sampled every 3 h. For the following experiments, we assign $\alpha = 1.2$, since it is preferable to use a value of α as small as possible to resolve the scale separation (Lacorata et al., 2001), and this is the smallest α in this set of experiments where λ is insensitive to the precise value of the parameter.

Focusing on the nearly identical curves of $\lambda(\delta) \geqslant 1.2$ in Fig. 2, we note the following. For scales larger than 20 km, the FSLE follows a power law $\lambda(\delta) \sim \delta^{-0.8}$. This super-diffusive regime is fairly consistent with $D^2(t) \sim t^{2.2}$ (which corresponds to $\lambda \sim \delta^{-0.9}$) seen in Fig. 2a. The two metrics, $D^2(t)$ and $\lambda(\delta)$ do not necessarily lead to identical results due to sampling differences (Lacorata et al., 2001; LaCasce and Ohlmann, 2003). The relative dispersion curve averages typically have increasing sample sizes for smaller separations, while the FSLE curves result from separation times averaged over larger numbers of particle pairs at larger scales. As such, the small discrepancy in scaling seen here appears satisfactory. The scaling relation for the model FSLE, $\lambda \sim \delta^{-0.8}$ for $\delta \geqslant 20$ km, is in very good agreement with $\lambda \approx \delta^{-0.84}$ in the range of $30 \leqslant \delta \leqslant 200$ km obtained by Lacorata et al. (2001, their Fig. 4) on the basis of trajectory data from 37 drifters launched in the Adriatic, although the values of λ for the synthetic trajectories are higher.

The Adriatic circulation is known to exhibit strong seasonality due, in part, to changes in the form of the prevailing wind stress. In order to assess the effect of seasonality on the relative dispersion and determine how representative any single-month analysis may be, we examine 8 months of available NCOM output. This includes three months in 2002 (non-assimilated) and five months of sea-surface temperature assimilating results from 2006. Fig. 3 displays 1-month records of $D^2(t)$ and $\lambda(\delta)$ for each of these 8 months. Note that in spite of the summer-fall predominance in the data set, the relative dispersion at all times and scales for March 2006 (winter–spring) and June 2006 (spring–summer) does not differ significantly from the other months. We obtain power laws of $D^2(t)$ varying between $t^{1.9}$ and $t^{2.3}$ (with an average $\sim t^{2.2}$) for $D_0 = 1$ km, and of $\lambda(\delta)$ between $\delta^{-0.8}$ and $\delta^{-0.9}$ (with an average of $\sim\delta^{-0.8}$) for $\delta > 20$ km. As seen in the FSLE curves, there are small but distinguishable differences between the data assimilating and non-data assimilating fields and a marked increase in the monthly variability within the data assimilating set. The relatively robust scaling indicates, however, that the dynamics which control the relative dispersion are present in all seasons, and in both configurations of the model.

Perhaps the most interesting aspect of any of the FSLE curves computed from the uniform $D_0 = 5.1$ km drifter array using all possible particle pair statistics is the lack of a clear exponential regime (constant $\lambda(\delta)$) at small separation scales. Such a plateau would be expected in any chaotic advection regime where the dispersion is dominated by

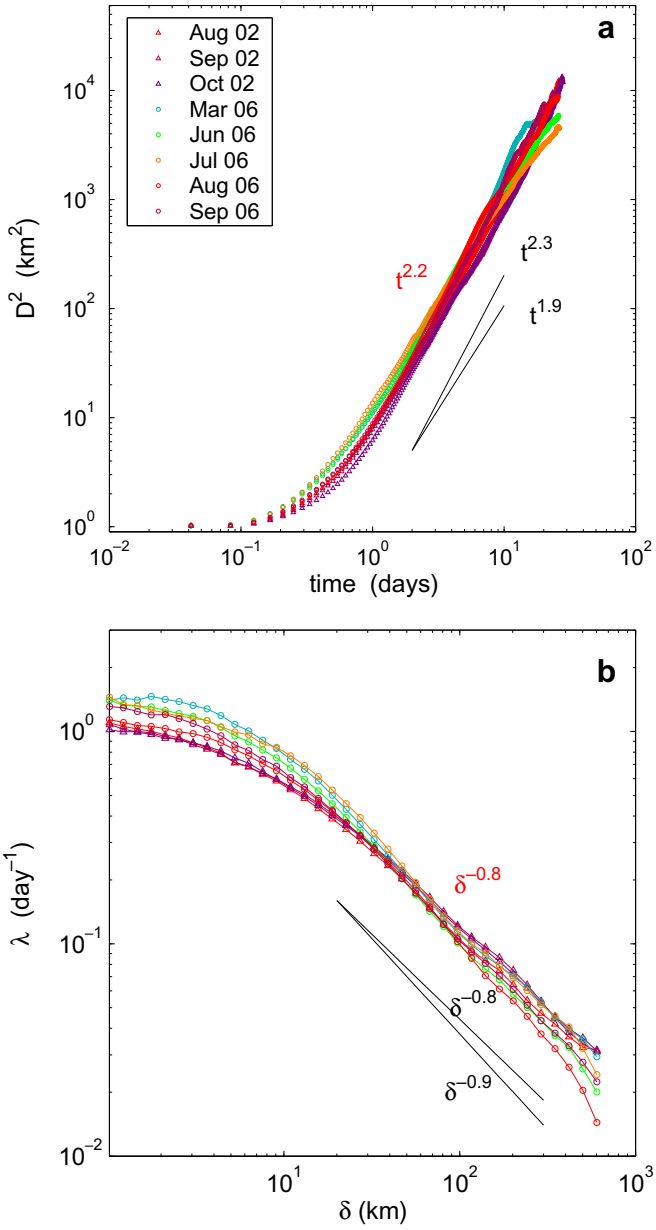

Fig. 3. (a) Relative dispersion $D^2(t)$ for $D_0 = 1$ km (chance pairs) and (b) FSLE $\lambda(\delta)$ curves for all available months in 2002 and 2006. The range in power laws is displayed by the black lines, while the average power law is indicated in red.

the time dependence of a spatially smooth velocity field. In the present context, however, there seems to be no clear law governing dispersion at scales in the range of $1 < \delta < 20$ km. The reasons for this almost surely involve the marked inhomogeneity in the Adriatic circulation and the dominating presence of the strong western boundary current. Strong differences in the statistics of 'interior' and 'boundary current' drifter pairs are coupled with the highly non-uniform rates at which these distinct regions are sampled by any initial distribution of drifters.

The effects of this are clearly seen in Fig. 4 where the differences between the $D_0 = 5.1$ km launch using all possible

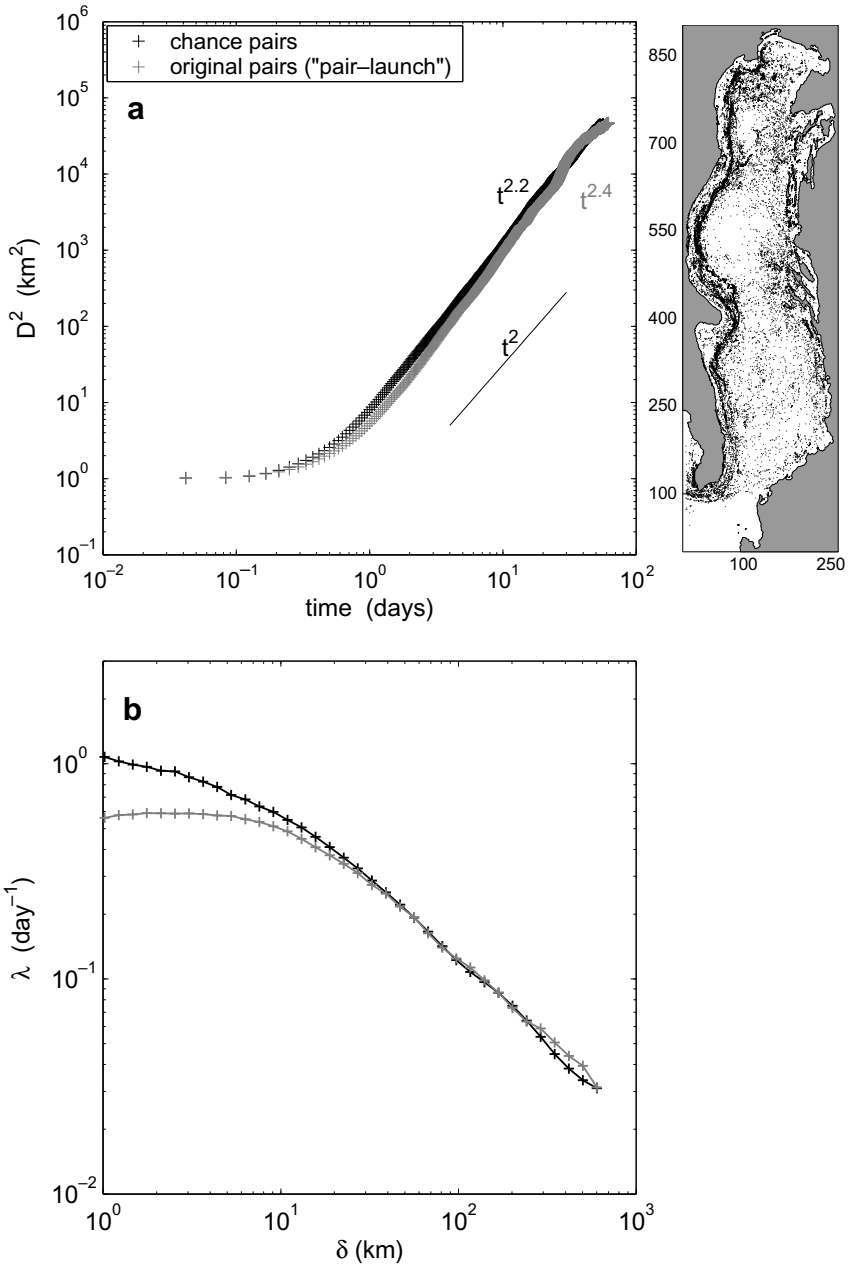

Fig. 4. (a) Total relative dispersion $D^2(t)$ with $D_0 = 1$ km computed from chance pairs (black crosses) and from the original pairs of the 'pair-launch' setting (gray crosses). (b) Corresponding FSLE curves for the two sampling strategies. Inset in upper figure shows the location of all chance pairs with $D_0 = 1$ km during the observation period.

particle pairs and the $D_0 = 1.0$ km launch using only the original pair statistics are compared for September 2002. In general, it is possible to calculate relative dispersion based not only on the particles that are launched together (so-called original pairs), but also based on those (so-called chance pairs) that approach one another at some later time (LaCasce and Bower, 2000). Chance pair sampling is typically employed to increase the sample size when only a limited number of drifter trajectories are available. This is usually the case in oceanic observations, but not a critical factor when synthetic drifter data can be generated from numerical model output. Nevertheless, using chance pairs, it is possible to calculate the time evolution of the relative dispersion of particles starting from smaller initial distances than those of the original pairs, namely down to the numerical model grid size of 1 km.

Fig. 4a shows that relative dispersion for the $D_0 = 1$ km pair-launch displays $D^2(t) \sim t^{2.4}$ which is somewhat steeper than that of the chance pair computation with larger initial separation, although the statistics at long times are considerably less robust in this case. More striking differences between the two sampling strategies are seen in the FSLE results shown in Fig. 4b. While the behavior is unchanged at scales larger than 20 km, the fixed sampling pair strategy

exhibits a distinct exponential regime at smaller scales. The reasons for this difference are apparent when one examines the spatial locations of all chance pairs approaching within $D_0 = 1$ km as shown in the inset of Fig. 4a. The inhomogeneity of the flow field and the lack of any ergodicity in the drifter trajectories implies that chance pairs with small separations occur with much higher frequency on the energetic boundaries of the Western Adriatic Current. At small scales, the chance pair statistics preferentially weight this flow feature. In contrast, fixing the number of particle pairs at the outset, as in the original pair strategy, preferentially weights less energetic interior gyre flow features which produce larger separation times.

The controlling effect of energetic WAC also explains the marked sensitivity of the computed FSLE curves to the choice of doubling parameter α. Choosing α too small effectively removes those particle pairs in the WAC which separate the smallest distances on time scales faster than the Δt imposed by the model archiving. As expected, averaged velocity differences computed from the Lagrangian structure function for the fixed pair launch are considerably less ($\Delta v \sim 1$ km/day at 1 km) than those computed from the chance pairs and the corresponding $\lambda(\delta)$ can be reliably computed with even smaller values of the doubling parameter, $\alpha_{\min}$.

The results in Fig. 4 indicate that the relative dispersion in the model Adriatic on scales <20 km is extremely sensitive to both the model resolution of the WAC and to how well this region is sampled by the Lagrangian drifters. The dynamics of the synthetic drifters at such scales are, in turn, dependent upon the details of the spatial and temporal interpolation schemes used. All processes at these scales are likely to be sensitive to the spatial and/or temporal accuracy of the model. Therefore, it is at these scales where one would anticipate the effect of the uncertainties by spatial and temporal smoothing to be most significant. In what follows, we restrict ourselves to the chance pair launch strategy which makes use of all possible drifter pair statistics from uniform launches of $N = 5172$ synthetic drifters. This choice provides large numbers of sample pairs at all scales while mimicking the observational reality of allowing the Lagrangian dynamics to control the location of individual drifter pairs at any time.

4.2. Effect of temporal averaging on relative dispersion

Having quantified relative dispersion and FSLE from the raw field, we now look at the effect of temporal averaging. First, snapshots of the flow field and synthetic trajectories are plotted in Fig. 5 in order to assess how averaging the Eulerian field impacts the drifter trajectories. Three levels of temporal filtering are employed: 1.5, 3, and 30 days. A 1.5-day filtering is commonly used for the removal of inertial oscillations exhibited by the drifter trajectories in the Adriatic Sea. The subset of trajectories after such filtering of the flow-field indeed shows that most of the loopers present in the Adriatic interior (Fig. 1b) have been eliminated (lower panel, Fig. 5b). We note that the 3-day moving average reduces by half the intensity of the anticyclonic eddy in the southern Adriatic, due to its propagation, while the overall structure of the boundary currents are fairly well preserved in the three smoothing cases. Eddies disappear almost entirely from the flow field in the case of 30-day temporal filtering. Similar considerations apply to other fast-moving events, while the quasi-permanent coherent features of the flow field remain after time averaging. Such a flow field leads to extremely smooth trajectories that are mainly confined to the boundary currents and exhibit significantly less zonal (cross-basin) transports. This implies that much of the zonal transport in this Adriatic Sea simulation is carried out by episodic events, such as meandering of the boundary currents, swirls, filaments, and eddies. As shown in Section 4.4, the meandering and eddying of the WBC is a major source of rapid, meso-scale and submeso-scale particle dispersion in the Adriatic basin.

The relative dispersion and FSLE curves for velocity fields subjected to temporal averaging are plotted in Fig. 6a and b, respectively. The curves from the raw fields are also shown for comparison. From both $D^2(t)$ and $\lambda(\delta)$, it is apparent that time-filtering influences the small-scale dispersion only. In the case of $D^2(t)$, the influence of the removal of time variability manifests itself by an increased delay for the onset of dispersion in the range of a few hours to 2 days. The small-scale, short-time dispersion is reduced. The large-scale dispersion remains unchanged from the super-diffusive regime of $D^2(t) \sim t^{1.9}$. In the case of the FSLE, the effect of time smoothing manifests itself by reduced dispersion (smaller FSLE) at scales in the range of 1–20 km, which essentially covers the submeso-scale and meso-scale variability that is filtered out. Dispersion at the smallest scale computed here, $\delta = 1$ km, is reduced by half using the monthly mean velocity field. As in $D^2(t)$, dispersion at larger scales remain unchanged, displaying $\lambda \sim \delta^{-0.8}$ for $\delta > 20$ km.

We note that the features of the circulation remaining in the mean flow are the boundary currents and basin-scale gyres after 30-day temporal smoothing (upper panel, Fig. 5c). We conclude that the mean boundary currents and persistent stretching at the interface between the basin gyres are actually the main circulation features controlling the dispersion at large scales. These features are not affected by the temporal filtering of the flow field. As such, the $D^2(t) \sim t^{1.9}$ or $\lambda(\delta) \sim \delta^{-0.8}$ regimes appear to be a consequence of horizontal shear dispersion and persistent isolated regions of high strain in the Eulerian field.

4.3. Effect of spatial smoothing on relative dispersion

The effect of spatial smoothing on the relative dispersion is investigated next by applying a Gaussian filter to the velocity field for different values of σ. The upper panel of Fig. 7 illustrates the progressive smearing of the circulation features with σ values of 2.5, 5, and 10 km. The internal

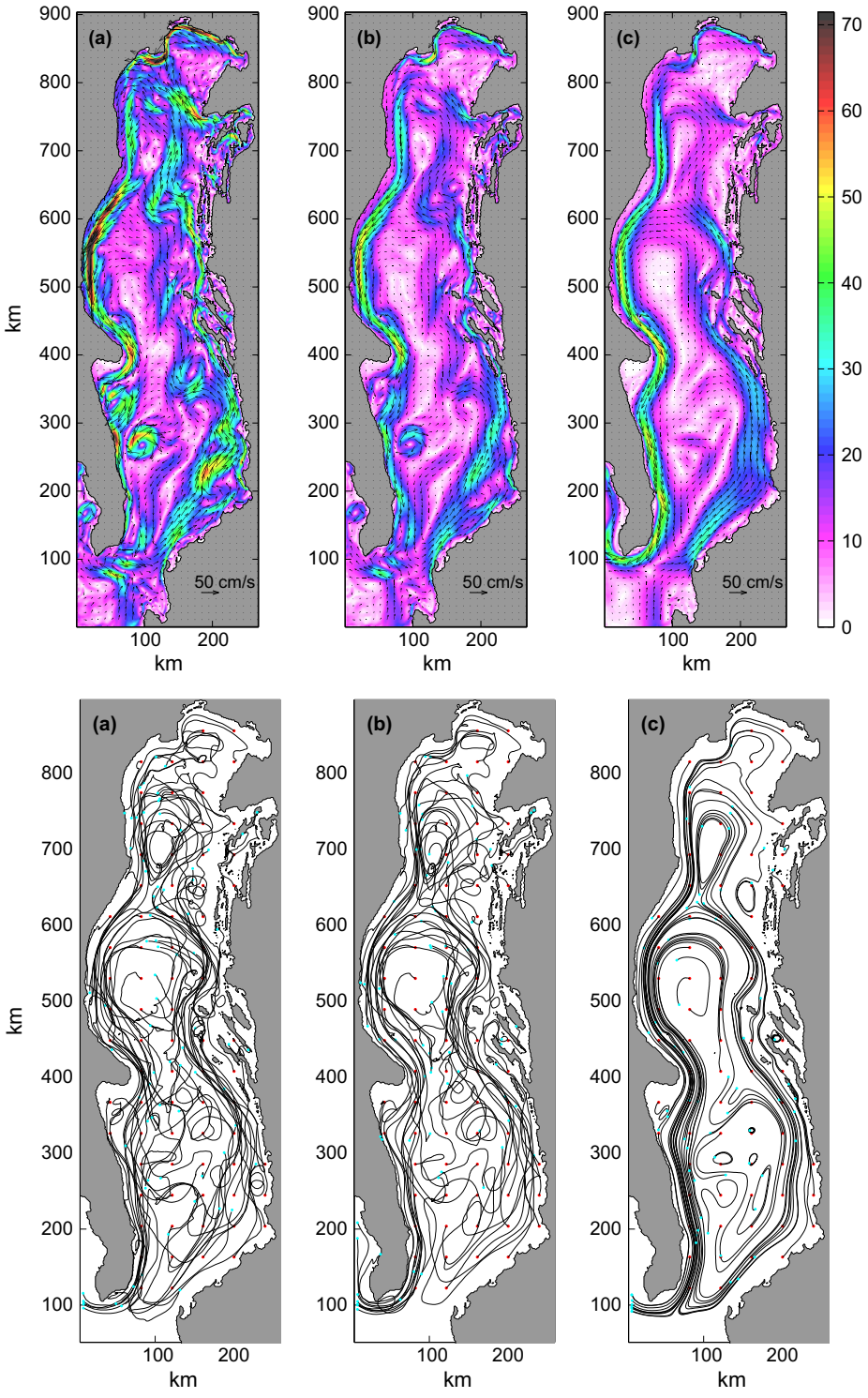

Fig. 5. Upper panel, snapshots of the surface velocity field after applying time smoothing with a window size of (a) 1.5 days, (b) 3 days, and (c) 30 days. The colors indicate the speed (in cm/s). Lower panel, trajectories of 74 synthetic drifters advected with the same low-pass filtered velocity fields.

deformation radius in the Adriatic can be as short as 5 km (Cushman-Roisin et al., 2007). As such, meso-scale features like the anticyclonic eddy downstream of the Gargano Cape are smoothed out with $\sigma = 10$ km and the boundary currents become wider and slower for larger values of σ.

The corresponding trajectories (lower panel, Fig. 7) show how different the effect of spatial filtering is from that of temporal filtering. The difference in the trajectories from the spatially filtered velocity fields and those from the raw field (Fig. 1b) is barely apparent; inertial oscillations are

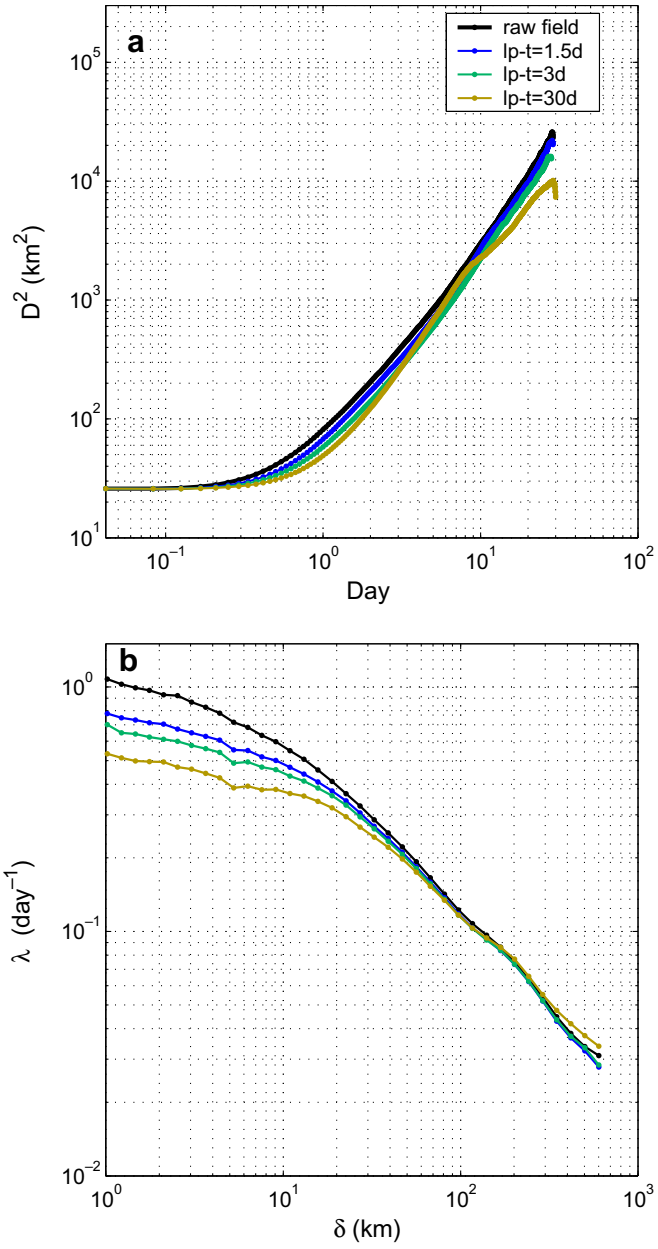

Fig. 6. (a) Relative dispersion $D^2(t)$ and (b) FSLE $\lambda(\delta)$ curves in cases of temporal low-pass filtering of the velocity field.

still present in the regions of low kinetic energy, even for large σ, and cross-basin transports remain virtually unmodified. The persistence of inertial oscillations is not surprising as their dynamical balance requires only time dependence of the underlying field and the effect of rotation.

D^2 and λ computed for six different values of σ ranging from 0.5 to 20 km are plotted in Fig. 8. For these cases, the trajectories of particles venturing too close to the coast were discarded to avoid the spurious dispersion generated by the spatial smearing of the surface boundary layer with adjacent model land points. A condition on a depth shallower than 20 m was sufficient for most of the Adriatic basin with the exception of the Croatian coast where the entire circulation around the islands was dismissed. The FSLE and relative dispersion of the full field were also recalculated under the same boundary conditions for consistency.

For $0.5 \leqslant \sigma \leqslant 5$ km, the spatial filtering acts on the relative dispersion in a similar way as the temporal filtering, by affecting mostly the scales below 10–20 km. In particular, $\sigma = 2.5$ km and 1.5-day low-pass filtering yield very similar curves. We conclude that spatial smoothing in this range eliminates fine-scale turbulent features that are also fast enough to be affected by the 1.5-day temporal filtering. As shown in Section 4.4, such small scale structures are predominantly associated with instabilities in the WAC and eddies within the Croatian island chain. Note also that the D^2 power law remains the same in this range of σ.

For $\sigma \geqslant 10$ km, the large-scale dispersion starts to be affected, which corresponds to the smearing of the WAC and EAC observed in Fig. 7c. The dispersion curves $D^2(t)$ for the large σ, as seen in Fig. 8a, no longer display a power law. The FSLE λ exhibits now an exponential-type regime for $5 \leqslant \delta \leqslant 20$ km. Therefore, it appears that spatial smoothing large enough to weaken the features of the mean flow influences relative dispersion at all scales. Relative dispersion tends to be dominated by chaotic advection at small scales since time variability is preserved and large-scale relative dispersion tends to decrease because of reduced horizontal shears in the boundary currents and weakening/elimination of high rate of strain regions throughout the domain.

4.4. Analysis

One of the striking results of these calculations is the robustness of the large-scale relative dispersion to temporal and spatial filtering of the velocity field, or in other words, the degree of control exerted by the large-scale circulation on the tracer evolution. We now provide arguments to help explain this finding based on both classical, namely energy cascade, and recent dynamical-system methods.

Bennett (1984) put forth the concept of two dynamical regimes: a local regime where the tracer evolution at a given length scale is controlled by the velocity field at the same length scale and a non-local regime where the tracer evolution is controlled by the velocity field at much larger scales. In particular, Bennett (1984) showed that the transition between the local and non-local regimes depends on the slope of the kinetic energy spectrum. When the slope is steeper than -3, then non-local control of the tracer field becomes dominant. While this analysis relies on the connection between the velocity structure function and the energy spectrum for homogeneous, isotropic turbulence, investigations by Babiano et al. (1985) and Shepherd et al. (2000) for derived atmospheric velocity data further support the result. While the Adriatic model produces a velocity field is distinctly inhomogeneous and non-isotropic, computations of the wave-number spectra (not shown)

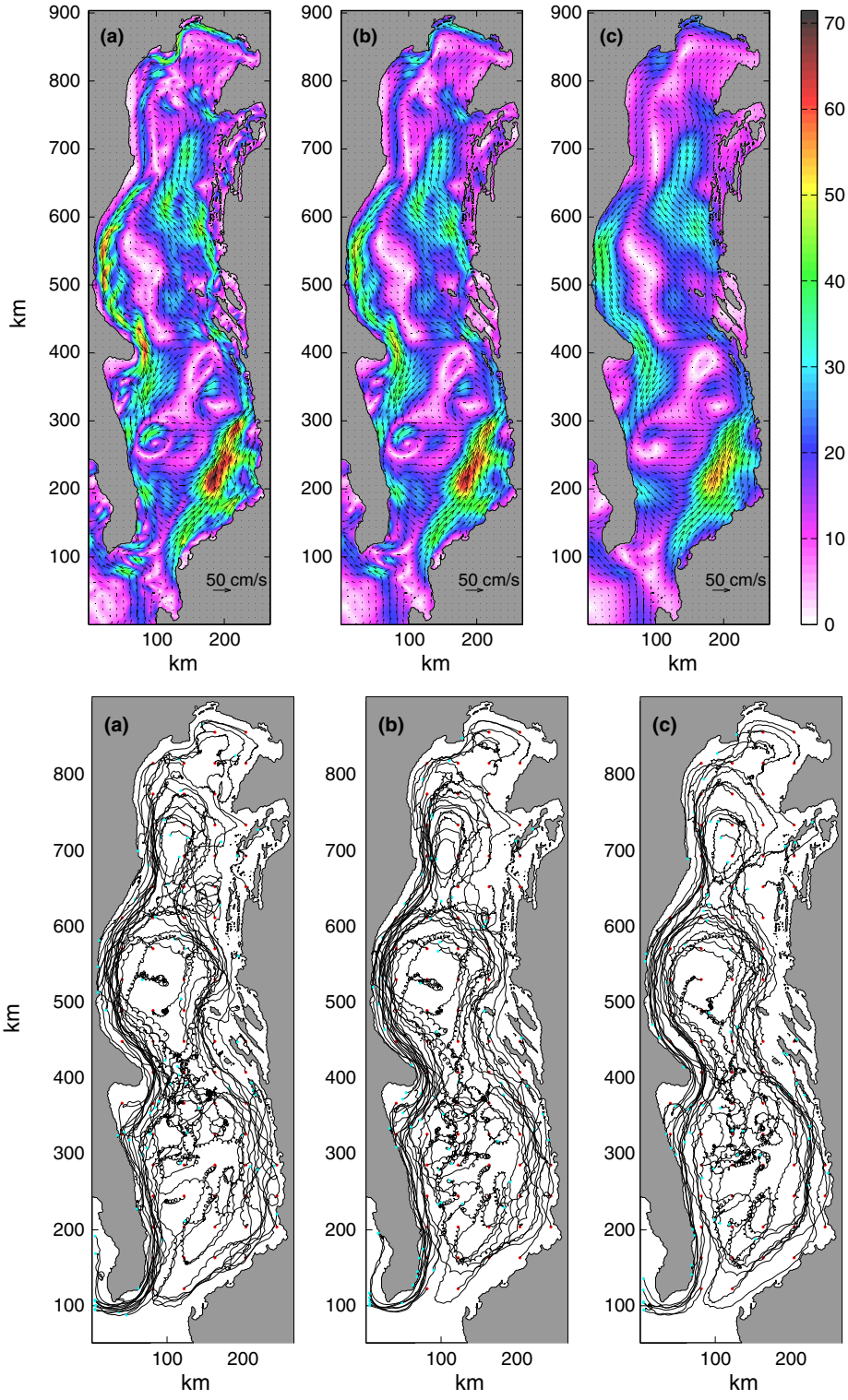

Fig. 7. Upper panel, snapshots of the surface velocity field after applying a Gaussian spatial filter with (a) $\sigma = 2.5$ km, (b) $\sigma = 5$ km, and (c) $\sigma = 10$ km. Lower panel, trajectories of 74 synthetic drifters advected with the same spatially filtered velocity fields.

indicate spectral slopes significantly steeper than k^{-3}. The observed 'non-local' behavior of the relative dispersion, dominated by the presence of highly sheared boundary currents and large-scale gyres, is at least not inconsistent with spectral predictions.

Next, we investigate the spatial distribution of the FSLEs and how temporal and spatial filtering affects this distribution. Maps of the distribution of FSLE for a fixed scale are often used to identify high-dispersion regions and mixing boundaries. In particular, the spatial distribution of

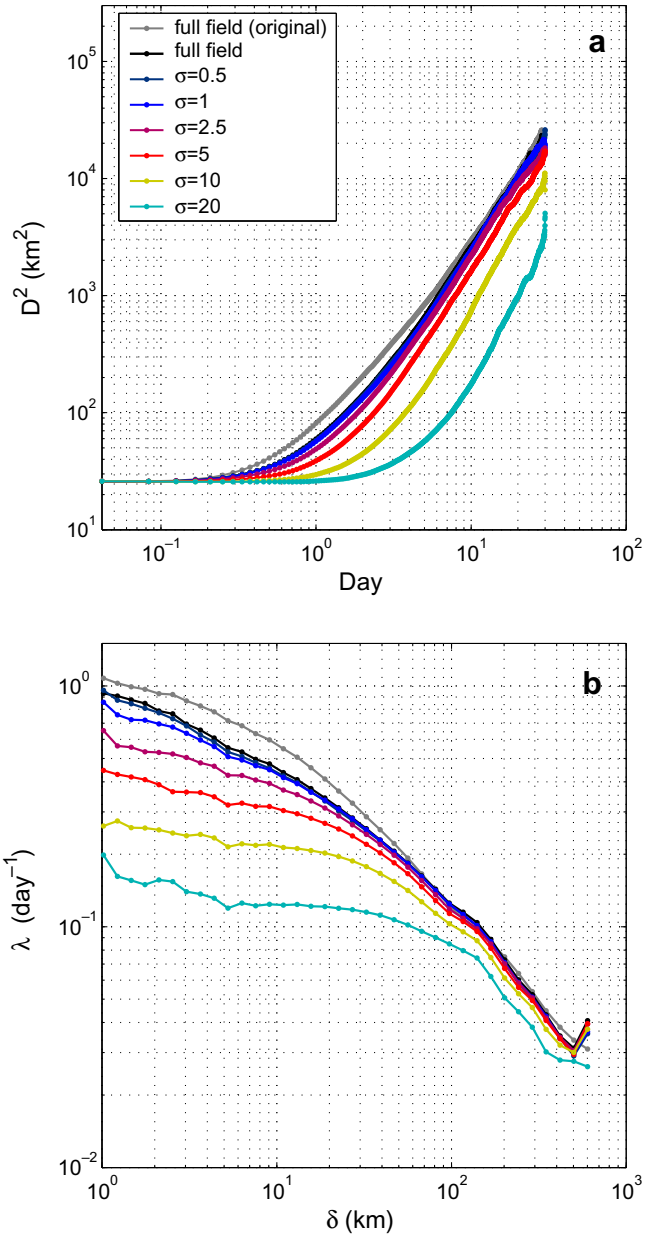

Fig. 8. Effect of space-smoothing on (a) the relative dispersion and (b) on the FSLE curve for six different values of σ. The trajectories near the coastline have been discarded to avoid spurious dispersion, and the difference in D^2 and λ is highlighted by the new (black) and original (gray) full field curves.

the Lagrangian structures can be identified by plotting FSLE maxima from forward and backward-in-time advection of synthetic drifters, as explained in d'Ovidio et al. (2004) and Molcard et al. (2005). To this end, the FSLE map corresponding to the model simulation on September 6, 2002 is calculated based on 6 days of forward and backward drifter advection using an initial pair distance of 0.45 km and $\alpha = 15$. This selection of parameters provides insight on the structure of fine-scale Lagrangian features, while allowing them time to fully emerge.

The spatial distribution of FSLE for the full model velocity field is plotted in Fig. 9a. The map clearly shows the inhomogeneity in the dispersion field and the confinement of rapid particle pair separations to a few distinct regions and isolated flow features. The vast majority of particle pairs undergoing rapid separation to scales of order 15–30 km initiate in confined regions along the WAC, in the Croatian islands, and at the boundaries of entraining or detraining eddies near inter-gyre boundaries and behind the Gargano Peninsula. The WAC is clearly a controlling influence on the overall relative dispersion in the Adriatic. The intense foliation of Lagrangian structures shown by the overlapping of FSLE maxima mark the complicated pathways by which Lagrangian parcels are entrained and detrained from the boundary current. In that sense, the tangle of the FSLE curves indicates the spatial extent of the fluctuations in the WAC and the transport among interacting, small-scale eddies there. Notably, a vanishingly small number of model particle pairs initiated in the gyre interiors separate to the modest $\alpha = 15$ scale in the 6-day integration period. The number of identifiable 'eddy' features external to the boundary currents as shown by isolated transverse intersections of forward and backward in time FSLE maxima is small. Three of the strongest are located in the southern gyre with another marked by the figure eight pattern near (200, 625) in grid-point units.

The main effect of the temporal filtering as shown in Fig. 9b–d, is to remove the tangling caused by the time-dependent eddies, filaments, and meandering of the WAC. The details of these structures are considerably changed for smoothing windows as short as 1.5 days. The other isolated eddy-mixing regions are longer lived and persist in the FSLE maps for 5-day and longer averaging times. What structure persists along the main edges of the WAC under time filtering can be identified with distinct regions of high strain rate in the mean field, for example, the mean separation bubble behind the Gargano peninsula and the flow around Isole Tremiti north of Gargano.

Another way of looking at this is by plotting the probability density distribution (pdf) of τ at different separation distances. Fig. 10 shows that at distances up to approximately 20 km, temporal filtering influences the pdf of τ such that the peak taking place at short times is reduced and the pdf moves to longer time scales (Fig. 10a). In contrast, temporal filtering has no impact on the pdf for larger scales (Fig. 10b). Thus, it is clear that while the complex fine-scale instabilities, eddies, and filaments in the surface velocity field control relative dispersion at scales smaller than the thickness of the boundary currents, ≈20 km, the shear along the edges of the boundary currents and persistent mean flow separation features entirely dictate the large-scale dispersion. As such, when these instabilities are smoothed out by time averaging, the small-scale dispersion is affected while large-scale relative dispersion remains intact.

On the other hand, the spatial filtering up to $\sigma \leqslant 5$ km (Fig. 9e–g) maintains the time-dependent component of the tangling of the Lagrangian structures, but reduces the intensity of local velocity gradients. The signatures of the

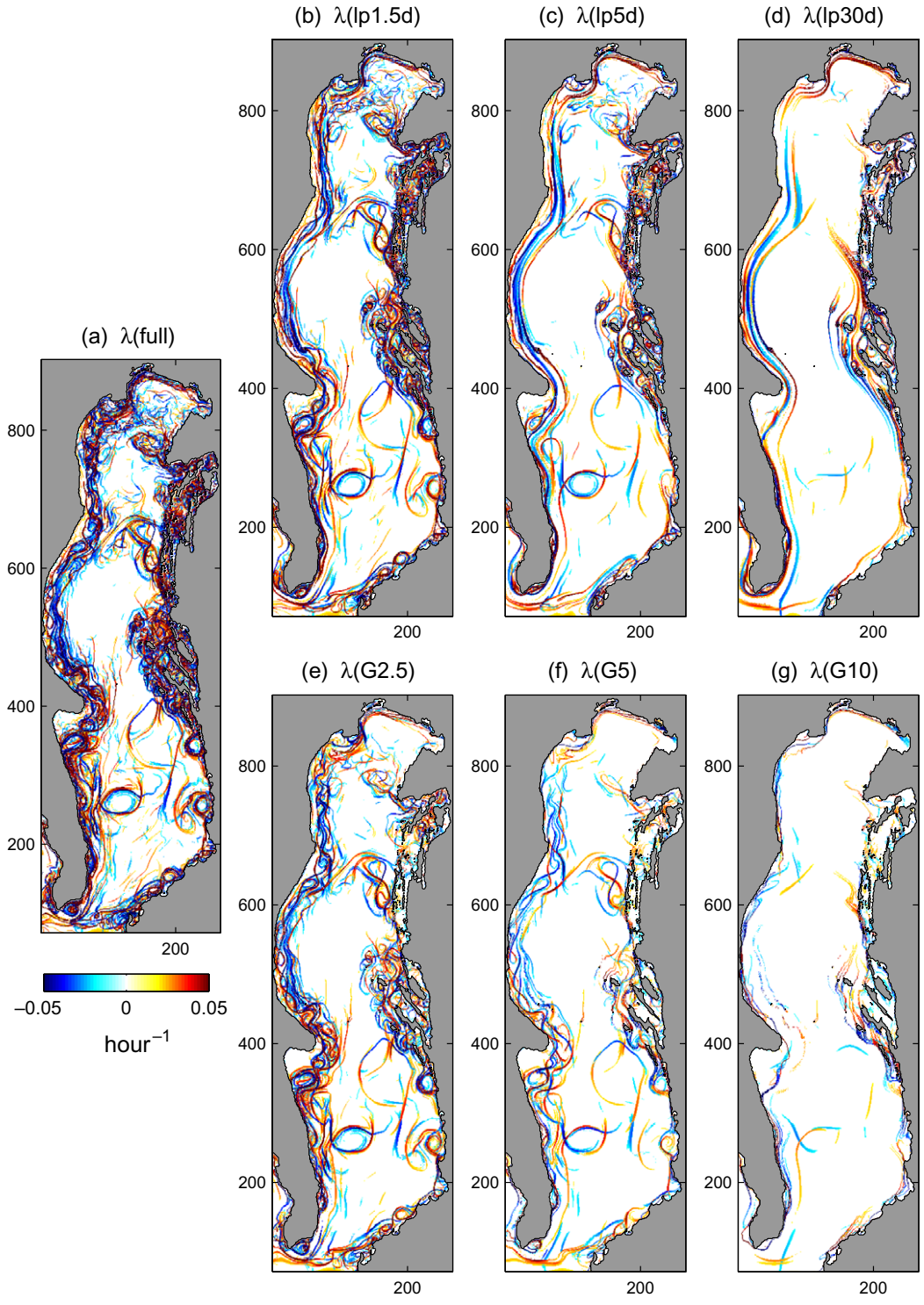

Fig. 9. Spatial distribution of FSLEs forward 6 days in time starting from September 6, 2002 (positive) and backward 6 days in time (negative) calculated with an initial pair distance of $\delta_0 = 0.45$ km, and $\alpha = 15$ (units are h^{-1}) from (a) the raw field, (b) with 1.5-day time filtering, (c) with 5-day time filtering, (d) with 30-days time filtering, (e) with spatial smoothing using $\sigma = 2.5$ km, (f) $\sigma = 5$ km, and (g) $\sigma = 10$ km.

WAC and corresponding eddies dissipate for $\sigma = 10$ km (Fig. 9f), as the overall sheer is reduced and spatially distinct separation regions are averaged out completely. The pdf of τ (Fig. 10c) behaves in a similar way for spatial filtering to temporal filtering for $\sigma \leqslant 10$ km. This is when small-scale turbulent structures are being eliminated from the flow field. But for larger σ values, the pdf changes significantly, with the peak moving toward longer times and decreasing in amplitude. This is due to the overall reduction in the velocity gradients responsible for fast disper-

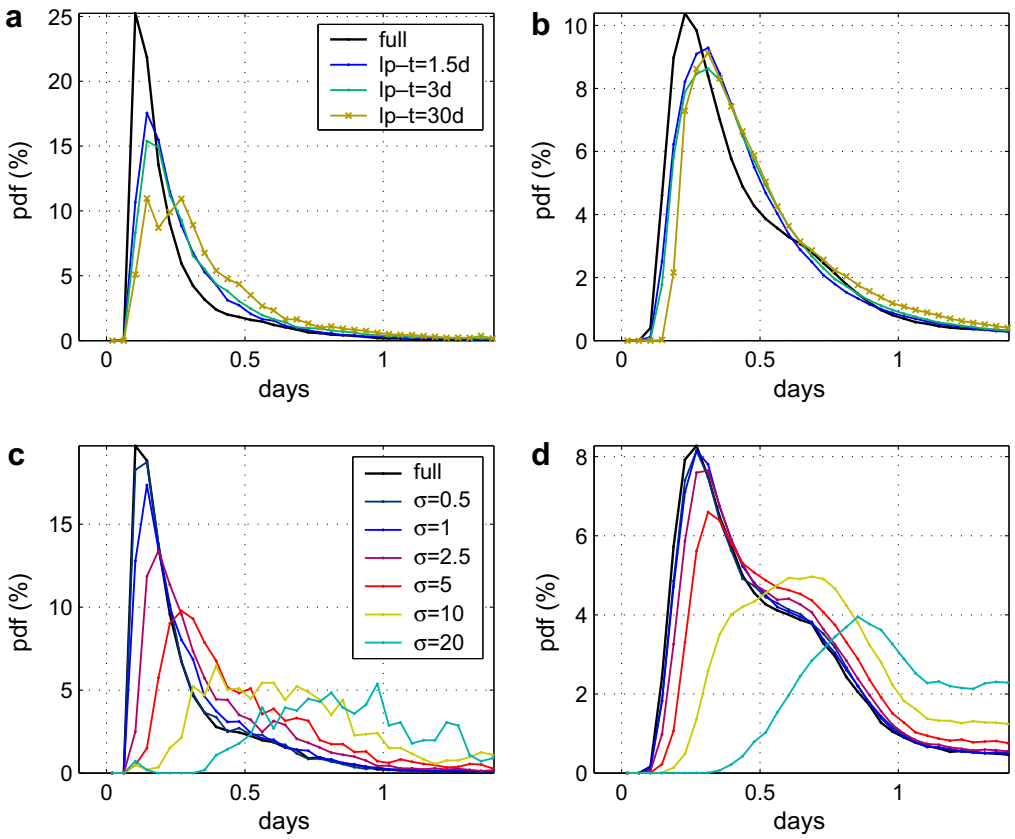

Fig. 10. Comparison of the distributions of dispersion times τ, defined as the time required for a particle pair to separate from δ to $\alpha\delta$, for the full and filtered velocity fields. Two separation distances are chosen to highlight the filtering effect on the different scales of the flow: (a) 2.1–2.5 km, temporal filtering, (b) 18.8–22.6 km, temporal filtering, (c) 2.1–2.5 km, spatial filtering, and (d) 18.8–22.6 km, spatial filtering.

sion. The data indicate that this occurs for averaging scales smaller than the width of the boundary currents (Fig. 10d). Once the isolated small-scale spatial structures and shear dispersion zones are eliminated, the remaining simpler flow field (lower panel, Fig. 7c) combined with time variability enforce an exponential regime in relative dispersion that is characteristic of chaotic advection (Fig. 8b).

A final set of experiments is carried out to further differentiate the roles played by persistent mean structures and time-dependent fluctuations. This is done by examining the relative dispersion statistics resulting solely from the time-dependent component of the flow produced by removing the monthly mean field. This fluctuating, or 'turbulent' field is given by $\mathbf{u}_t(\mathbf{x},t) = \mathbf{u}(\mathbf{x},t) - \overline{\mathbf{u}(\mathbf{x})}$, where $\overline{\mathbf{u}(\mathbf{x},t)}$ is the monthly mean velocity.

As discussed, low-pass temporal filtering results indicate that the large-scale relative dispersion is dominated by mean shear zones concentrated in the boundary currents. The procedure of removing the mean flow is therefore similar to a high-pass filtering in this case (albeit not equivalent, since there may still be large scale residuals from the boundary currents). One would expect the results to be significantly different with respect to those obtained from temporal low-pass filtering. The resulting dispersion and FSLE curves are plotted in Fig. 11, and display behaviors remarkably opposite to the low-pass experiments: both D^2 and λ are identical to the full flow dispersion at small temporal ($t < 2$ days) and spatial ($\delta < 5$ km) scales, while the dispersion at larger scales changes. This is indeed the only experiment where the relative dispersion at scales smaller than the radius of deformation remains unchanged. Therefore, the results indicate that the shear in the mean flow does not play a role in the dispersion at small scales. After 20 days, D^2 approaches a power law of $D^2 \sim t^{1.5}$, and a diffusive regime after 1 month. The FSLE at scales beyond 20 km displays a pure ballistic regime $\lambda \sim \delta^{-1.0}$. While D^2 and λ differ regarding the dispersion laws, both metrics show that when persistent mean flow structures are removed, the relative dispersion is considerably slowed at large temporal and spatial scales. The distinct ballistic regime observed in the FSLE at meso- and larger-scales can be attributed to a highly organized fluctuating velocity field characterized by long correlation times.

5. Summary and conclusions

Quantification of relative dispersion is important for practical problems in geophysical fluid dynamics and is a classical area of study in fluid mechanics. Several regimes of relative dispersion have been identified on a theoretical

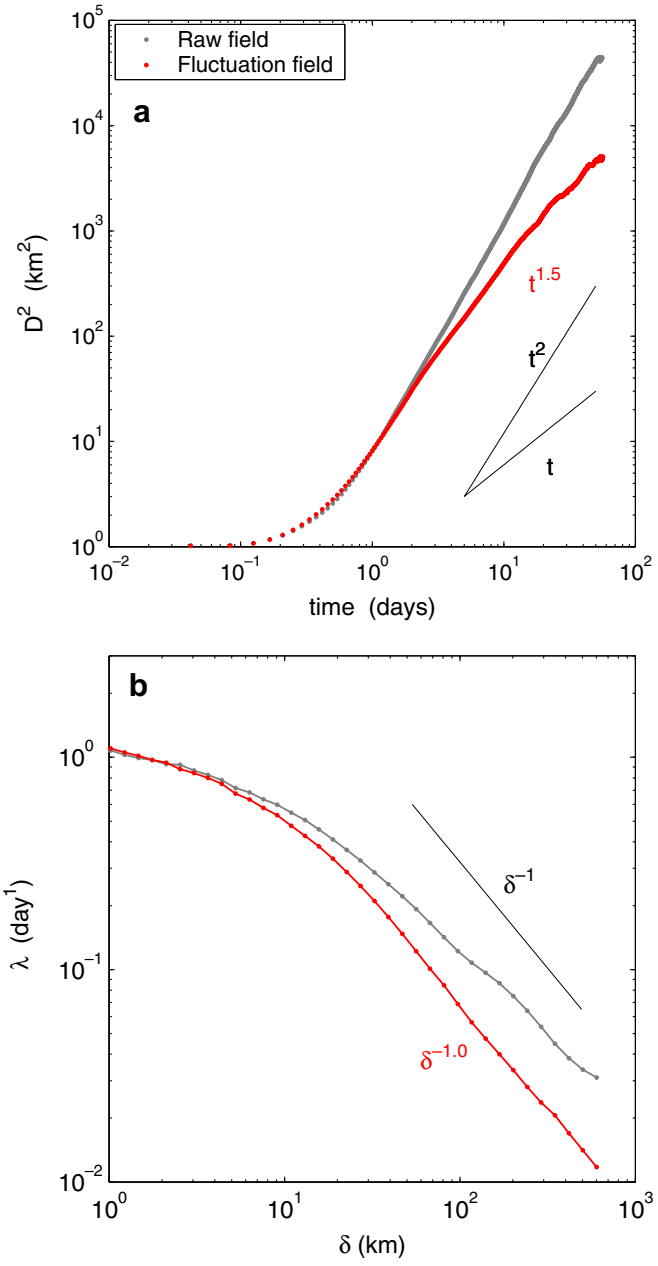

Fig. 11. (a) Relative dispersion $D^2(t)$ and (b) FSLE $\lambda(\delta)$ curves in the case of detrended velocity field.

basis for canonical turbulent flows, but it remains unclear to what extent these regimes are realized in the ocean and, in particular, in complex coastal flows. Investigation of relative dispersion in the ocean has been traditionally limited by the limited number of drifter pairs launched with small initial separations. Recent advances in the realism of coastal and ocean circulation models allow investigation of relative dispersion based on synthetic drifters.

Our main objective is to study relative dispersion in the Adriatic Sea circulation using an ocean model that employs not only very high spatial and temporal resolution, but is also driven by realistic surface, tidal, river, and boundary forcing. The Adriatic is a semi-enclosed (marginal) sea, the circulation of which is characterized by strong boundary currents and interior gyres. The surface flows in the Adriatic Sea are subject to strong wind forcing that is modulated by the surrounding land topography. The buoyancy input by the Po and other rivers leads to a strong WAC, and its baroclinic instabilities are known to facilitate the formation of eddies and filaments that should presumably be very important for relative dispersion at the meso-scale range. As such, the Adriatic is an interesting and challenging place to explore this problem. Relative dispersion in the Adriatic Sea has been subject to prior investigation by Lacorata et al. (2001) using 37 real drifters and an idealized kinematic numerical model. A secondary objective of this study is to quantify the impact of the uncertainties that can arise from numerous errors in the numerical modeling and/or forcing data on the resulting Lagrangian statistics. This is done simply by applying temporal and spatial filtering to the model Eulerian velocity fields.

Relative dispersion based on the raw model data shows $D^2(t) \sim t^{\gamma}$, where $\gamma = 1.9$ using original pairs with $D_0 = 5.1$ km, and $\gamma = 2.2$ using chance pairs with $D_0 = 1$ km for $t \geqslant 10$ days (a different type of launch using chance pairs with $D_0 = 1$ km yields $\gamma = 2.4$), while the FSLE shows $\lambda \sim \delta^{-0.8}$ (corresponding to $D^2(t) \sim t^{2.5}$) for $\delta \geqslant 20$ km. As such, a super-diffusive relative dispersion is documented at these scales that is close to ballistic based on $D^2(t)$ and between the ballistic and Richardson's regimes based on the FSLE. The value $\lambda \sim \delta^{-0.8}$ is in very good agreement with results from Lacorata et al. (2001) based on real drifters. At smaller spatial (and faster temporal) scales, no clear dispersion law is detected, in particular, an exponential regime characteristic of chaotic advection and/or enstrophy cascade is not realized. Analysis of NCOM output from additional months and a different year of simulation show no significant change in the scaling laws, which indicates that the flow features responsible for the overall relative dispersion persist across seasons. Nevertheless, it should be noted that seasonality is computed based on chance-pairs. This approach undersamples the regions of relatively lower activity which are possibly more sensitive to the wind regimes and thus to the seasonal variability of the forcings.

Temporal filtering of the velocity field with a time window up to 30 days only affects relative dispersion at scales smaller than 20 km by reducing their rate of dispersion by half. Relative dispersion at scales larger than 20 km remains intact. In contrast, spatial smoothing with a Gaussian filter with σ up to 20 km affects dispersion at almost all scales of motion. The primary difference between temporal and spatial smoothing is that spatial smoothing modifies the coherent structures of the mean flow field, in particular, the shear in the boundary currents for smoothing at the scale of these currents. As such, we conclude that large-scale relative dispersion is mainly controlled by the mean flow in the Adriatic Sea. The control exerted by the large-scale flow on the tracer evolution is, at least, not

inconsistent with the ideas put forth by Bennett (1984) in that the slope of the kinetic energy spectrum is steeper than −3 although the model velocity is far removed from any traditional turbulence.

Relative dispersion at scales smaller than 20 km and 10 days shows no clear fit to the traditional ideas and both the overall statistics and spatial structure are found to be extremely sensitive to the resolution and sampling of the WAC region. When spatial smoothing is strong enough to weaken the influence of shear dispersion from the boundary currents, the remaining regime appears to be dominated by chaotic advection. This implies that all chaotic advection, shear dispersion, and small-scale turbulent features such as filaments and eddies play a role in relative dispersion at these scales. Since these scales are the most important for environmental problems with societal impact, we conclude that relative dispersion at these scales should be most effectively attacked by using very realistic, high-resolution ocean models. The accuracy of these models needs to be tested and improved using observations at submeso-scales.

Acknowledgements

We are grateful to ONR via Grants N00014-05-1-0094 and N00014-05-1-0095 (Haza, Özgökmen), N00014-00-0019 (Poje), Program Element 0602435 (Martin), and to NSF via ATM-200102 (Poje). Thanks to Jim Doyle of NRL for supplying the COAMPS atmospheric forcing for the ocean simulations. Thanks to Rich Signell of the US Geological Survey for providing the Po discharge data. Also two anonymous reviewers contributed to a significant improvement of the manuscript.

References

Abraham, E.R., Bowen, M.M., 2002. Chaotic stirring by a mesoscale surface-ocean flow. Chaos 12, 373–381.

Aref, H., 1984. Stirring by chaotic advection. J. Fluid Mech. 192, 115–173.

Artale, V., Boffetta, G., Celani, A., Cencini, M., Vulpiani, A., 1997. Dispersion of passive tracers in closed basins: beyond the diffusion coefficient. Phys. Fluids 9 (11), 3162–3171.

Aurell, E., Boffetta, G., Crisanti, A., Paladin, G., Vulpiani, A., 1997. Predictability in the large: an extension of the concept of Lyapunov exponent. J. Phys. A 30, 1–26.

Babiano, A., Basdevant, C., Sadourny, R., 1985. Structure functions and dispersion laws in two-dimensional turbulence. J. Atmos. Sci. 42 (9), 941–949.

Barron, C.N., Kara, A.B., Hurlburt, H.E., Rowley, C., Smedstad, L.F., 2004. Sea surface height predictions from the global Navy Coastal Ocean Model (NCOM) during 1998–2001. J. Atmos. Oceanic Technol. 21 (12), 1876–1894.

Barron, C.N., Kara, A.B., Martin, P.J., Rhodes, R.C., Smedstad, L.F., 2006. Formulation, implementation and examination of vertical coordinate choices in the global Navy Coastal Ocean Model (NCOM). Ocean Modell., doi:10.1016/j.ocemod.2005.01.004.

Batchelor, G.K., 1952. Diffusion in a field of homogeneous turbulence II. The relative motion of particles. Proc. Cambridge Philos. Soc. 48, 345–362.

Bennett, A.F., 1984. Relative dispersion – local and nonlocal dynamics. J. Atmos. Sci. 41 (11), 1881–1886.

Bennett, A.F., 1987. A Lagrangian analysis of turbulent-diffusion. Rev. Geophys. (4), 799–822.

Berloff, P.S., McWilliams, J.C., Bracco, A., 2002. Material transport in oceanic gyres, part I: phenomenology. J. Phys. Oceanogr. 32, 764–796.

Berloff, P.S., McWilliams, J.C., 2002. Material transport in oceanic gyres, part II: hierarchy of stochastic models. J. Phys. Oceanogr. 32, 797–830.

Blumberg, A.F., Mellor, G.L., 1987. A description of a three-dimensional coastal ocean circulation model. In: Heaps, N. (Ed.), Three-Dimensional Coastal Ocean Models. American Geophysical Union, New York, NY, p. 208.

Boffetta, G., Celani, A., 2000. Pair dispersion in turbulence. Physica A 280 (1–2), 1–9.

Boffetta, G., Sokolov, I.M., 2002. Relative dispersion in fully developed turbulence: the Richardson's Law and intermittency corrections. Phys. Rev. Lett. 88 (9), 4.

Boffetta, G., Celani, A., Cencini, M., Lacorata, G., Vulpiani, A., 2000. Nonasymptotic properties of transport and mixing. Chaos 10 (1), 50–60.

Bourgoin, M., Ouellette, N.T., Xu, H., Berg, J., Bodenschatz, E., 2006. The role of pair dispersion in turbulent flow. Science 311 (5762), 835–838.

Bracco, A., von Hardenberg, J., Provenzale, A., Weiss, J.B., McWilliams, J.C., 2004. Dispersion and mixing in quasigeostrophic turbulence. Phys. Rev. Lett. 23, 084501.

Cardoso, O., Gluckmann, B., Parcollet, O., Tabelling, P., 1996. Dispersion in a quasi-two-dimensional-turbulent flow: an experimental study. Phys. Fluids 8 (1), 209–214.

Cushman-Roisin, B., 1995. Introduction to Geophysical Fluid Mechanics. Prentice-Hall, Englewood Cliffs, NJ, 320 pp.

Cushman-Roisin, B., Gacic, M., Poulain, P.M., Artegiani, A., 2001. Physical Oceanography of the Adriatic Sea: Past, Present and Future. Springer, New York, 304 pp.

Cushman-Roisin, B., Korotenko, K.A., Galos, C.E., Dietrich, D.E., 2007. Simulation and characterization of the Adriatic Sea mesoscale variability. J. Geophys. Res. 12, C03S14, doi:10.1029/2006JC003515.

d'Ovidio, F., Fernandez, V., Hernandez-Garcia, E., Lopez, C., 2004. Mixing structures in the mediterranean sea from finite-size Lyapunov exponents. Geophys. Res. Lett. 31, L17203, doi:10.1029/2004GL020328.

Egbert, G.D., Erofeeva, S.Y., 2003. Efficient inverse modeling of barotropic ocean tides. J. Atmos. Oceanic Technol. 19, 183–204.

Er-El, J., Peskin, R.I., 1981. Relative diffusion on constant level ballons in the Southern hemisphere. J. Atmos. Sci. 38, 2264–2274.

Falco, P., Griffa, A., Poulain, P.M., Zambianchi, E., 2000. Transport properties in the Adriatic Sea as deduced from drifter data. J. Phys. Oceanogr. 30 (8), 2055–2071.

Flather, R.A., Proctor, R., 1983. Prediction of North Sea Storm Surges using Numerical Models: Recent Developments in the UK. In: Sundermann, J., Lenz, W. (Eds.), North Sea Dynamics. Springer, New York.

Haza, A.C., Griffa, A., Martin, P., Molcard, A., Özgökmen, T.M., Poje, A.C., Barbanti, R., Book, J.W., Poulain, P.M., Rixen, M., Zanasca, P., 2007. Model-based directed drifter launches in the Adriatic Sea: results from the DART experiment. Geophys. Res. Lett., 34, doi:10.1029/2007GL029634.

Hodur, R.M., 1997. The Naval Research Laboratory's Coupled Ocean/Atmosphere Mesoscale Prediction System (COAMPS). Mon. Wea. Rev. 125, 1414–1430.

Holland, W.R., Chow, J.C., Bryan, F.O., 1998. Application of a third-order upwind scheme in the NCAR Ocean Model. J. Clim. 11, 1487–1493.

Huber, M., McWilliams, J.C., Ghil, M., 2001. A climatology of turbulent dispersion in the troposphere. J. Atmos. Sci. 58, 2377–2394.

Iudicone, D., Lacorata, G., Rupolo, V., Santoleri, R., Vulpiani, A., 2002. Sensitivity of numerical tracer trajectories to uncertainties in OGCM velocity fields. Ocean Modell. 4 (3), 313–325.

Julien, M.C., 2003. Dispersion of passive tracers in the direct enstrophy cascade: experimental observations. Phys. Fluids 15 (18), 2228–2237.

Kolmogorov, A.N., 1941. Dissipation of energy in a locally isotropic turbulence. Doklady Akad. Nauk SSSR 32, 141 (English translation 1991). Proc. Roy. Soc. London A434, 15–17.

Kraichnan, R.H., 1967. Inertial ranges in two-dimensional turbulence. Phys. Fluids 10, 1417–1423.

LaCasce, J.H., Bower, A., 2000. Relative dispersion in the subsurface North Atlantic. J. Mar. Res. 58, 863–894.

LaCasce, J.H., Ohlmann, C., 2003. Relative dispersion at the surface of the Gulf of Mexico. J. Mar. Res. 61 (3), 285–312.

Lacorata, G., Aurell, E., Vulpiani, A., 2001. Drifter dispersion in the Adriatic Sea: Lagrangian data and chaotic model. Ann. Geophys. 19, 121–129.

Lacorata, G., Aurell, E., Legras, B., Vulpiani, A., 2004. Evidence of a $k^{-5/3}$ Spectrum in the EOLE Lagrangian ballons in the low stratosphere. J. Atmos. Sci. 61, 2936–2942.

Lesieur, M., 1997. Turbulence in Fluids, third ed. Kluwer Academic Publishers, Dordrecht, 515 pp.

Lin, J.T., 1972. Relative dispersion in the enstrophy-cascading inertial range of homogeneous two-dimensional turbulence. J. Atmos. Sci. 29, 394–396.

Martin, P.J., 2000. A Description of the Navy Coastal Ocean Model Version 1.0. NRL Report NRL/FR/7322-00-9962, Naval Research Laboratory, SSC, MS 39529, 42 pp.

Martin, P.J., Book, J.W., Doyle, J.D., 2006. Simulation of the northern Adriatic circulation during winter 2003. J. Geophys. Res. 111, C03S12, doi:10.1029/2006/JC003511.

Maurizi, A., Griffa, A., Poulain, P.M., Tampieri, F., 2004. Lagrangian turbulence in the Adriatic Sea as computed from drifter data: effects of inhomogeneity and nonstationarity. J. Geophys. Res. 109 (C4), C04010.

Mellor, G.L., 1991. An equation of state for numerical models of oceans and estuaries. J. Atmos. Ocean Technol. 8, 609–611.

Mellor, G.L., Yamada, T., 1974. A hierarchy of turbulence closure models for planetary boundary layers. J. Atmos. Sci. 31, 1791–1806.

Molcard, A., Poje, A.C., Özgökmen, T.M., 2005. Directed drifter launch strategies for Lagrangian data assimilation using hyperbolic trajectories. Ocean Modell. 12, 268–289.

Morel, P., Larcheveque, M., 1974. Relative dispersion of constant level ballons in the 200-mb general circulation. J. Atmos. Sci. 31, 2189–2196.

Morey, S.L., Martin, P.J., O'Brien, J.J., Wallcraft, A.A., Zavala-Hidalgo, J., 2003. Export pathways for river discharged fresh water in the Northern Gulf of Mexico. J. Geophys. Res. 108 (1), 1–15.

Olascoaga, M.J., Rypina, I.I., Brown, M.G., Beron-Vera, F.J., Koçak, H., Brand, L.E., Halliwell, G.R., Shay, L.K., 2006. Persistent transport barrier on the West Florida Shelf. Geophys. Rev. Lett. 33, 22603, doi:10.1029/2006GL027800.

Ollitrault, M., Gabillet, C., DeVerdiere, A.C., 2005. Open ocean regimes of relative dispersion. J. Fluid Mech. 533, 381–407.

Orlanski, I., 1976. A simple boundary condition for unbounded hyperbolic flows. J. Comput. Phys. 21, 251–269.

Piterbarg, L.I., 2005. Relative dispersion in 2D stochastic flows. J. Turb. 6 (4), 1–19.

Poulain, P.M., 1999. Drifter observations of surface circulation in the Adriatic Sea between December 1994 and March 1996. J. Mar. Sys. 20 (1–4), 231–253.

Poulain, P.M., 2001. Adriatic Sea surface circulation as derived from drifter data between 1990 and 1999. J. Mar. Sys. 29 (1–4), 3–32.

Provenzale, A., 1999. Transport by coherent barotropic vortices. Ann. Rev. Fluid Mech. 31, 55–93.

Pullen, J., Doyle, J.D., Hodur, R., Ogston, A., Book, J.W., Perkins, H., Signell, R., 2003. Coupled ocean-atmosphere nested modeling of the Adriatic Sea during winter and spring 2001. J. Geophys. Res. 108 (C10), 3320, doi:10.1029/2003JC001780. rivers, Technical Report RF 02/94, Consiglio Nazionale delle Ricerche Insituto Sperimentale Talassografico, Trieste, Italy, 8 pp..

Raicich, F., 1996. On the fresh water balance of the Adriatic Sea. J. Mar. Syst. 9 (3–4), 305–319.

Richardson, L.F., 1926. Atmospheric diffusion shown on a distance-neighbor graph. Proc. Roy. Soc. London A 110, 709–737.

Rosmond, T.E., Teixeira, J., Peng, M., Hogan, T.F., Pauley, R., 2002. Navy Operational Global Atmospheric Prediction System (NOGAPS): forcing for ocean models. Oceanography 15, 99–108.

Sawford, B., 2001. Turbulent relative dispersion. Ann. Rev. Fluid Mech. 33, 289–317.

Shadden, S.C., Lekien, F., Marsden, J.E., 2005. Definition and properies of Lagrangian coherent structures from finite-time Lapunov exponents in two-dimensional aperiodic flows. Physica D 212, 271304.

Shepherd, T.G., Koshyk, J.N., Ngan, K., 2000. On the nature of large-scale mixing in the stratosphere and mesosphere. J. Geophys. Res. 105, 12433–12446.

Taylor, G.I., 1921. Diffusion by continuous movements. Proc. London Math. Soc. 2 (20), 196–212.

Waugh, D.W., Abraham, E.R., Bowen, M.M., 2006. Spatial variations of stirring in the surface ocean: a case study of the Tasman Sea. J. Phys. Oceanogr. 36, 526–542.

Wiggins, S., 2005. The dynamical systems approach to Lagrangian transport in oceanic flows. Ann. Rev. Fluid Mech. 37, 295–328.